

Submitted to Astronomical Journal

Dynamical Zodiacal Cloud Models Constrained by High Resolution Spectroscopy of the Zodiacal Light

S. I. Ipatov

*Astronomy Department, University of Maryland, College Park, MD 20742, USA; Space
Research Institute, Moscow, Russia*

siipatov@hotmail.com

A. S. Kuttyrev

NASA/GSFC, Greenbelt, MD 20771

G. J. Madsen¹

Anglo-Australian Observatory, P.O. Box 296, Epping, NSW 1710, Australia

J. C. Mather, S. H. Moseley

NASA/GSFC, Greenbelt, MD 20771

and

R. J. Reynolds

*Department of Astronomy, 475 North Charter st., University of Wisconsin at Madison,
Madison, WI 53706*

ABSTRACT

We present simulated observations of the Doppler shifts of the solar Mg I Fraunhofer line scattered by asteroidal, cometary, and trans-Neptunian dust particles. The studies are based on the results of integrations of orbital evolution of particles under the gravitational influence of planets, the Poynting-Robertson drag, radiation pressure, and solar wind drag. The derived shifts in the centroid and profile of the line with solar elongation are different for different sources of

¹NSF Distinguished International Postdoctoral Research Fellow

dust. A comparison of the velocities of zodiacal dust particles based on these numerical integrations with the velocities obtained from WHAM observations shows that the fraction of cometary dust particles among zodiacal dust particles is significant and can be dominant. A considerable fraction of trans-Neptunian dust particles among zodiacal dust particles also fits different observations. The mean eccentricity of zodiacal dust particles is estimated to be about 0.5.

Subject headings: zodiacal cloud — migration — dust particles — spectroscopy

1. Introduction

Ground-based spectroscopic observations allow one to study Doppler shifts of scattered solar Fraunhofer lines in the zodiacal light (e.g., James 1969, Hicks et al. 1974, Fried 1978, and East & Reay 1984). Analysis of these shifts thus provide an opportunity to explore velocities of interplanetary dust in the inner solar system. Using the Wisconsin H-Alpha Mapper (WHAM) spectrometer, Reynolds et al. (2004) were the first to obtain accurate measurements of the centroid velocities and line profiles of the scattered solar Mg I $\lambda 5184$ absorption line in the zodiacal light, both along the ecliptic equator and at high ecliptic longitudes.

The models for migration of dust particles are discussed in Section 2. These results are based on integrations of the orbital evolution of dust particles developed by Ipatov et al. (2004) and Ipatov & Mather (2006a-b) (all our recent papers can be found at astro-ph and at <http://www.astro.umd.edu/~ipatov>). In Sections 3 and 4, based on the results of our runs, we consider our model calculations of the radial velocity profile of the scattered Mg I line. We compare plots of centroid velocities and line widths of the Mg I line versus solar elongation with WHAM observations obtained by Reynolds et al. (2004). Studies of typical eccentricities and inclinations of zodiacal dust particles that fit the WHAM observations are presented in Section 5. In previous papers, observations have been compared with analytical models, but this is the first comparison with numerical integrations of the particles.

2. Models for Migration of Dust Particles

Our studies of the Mg I line shifts use the results of following the orbital evolution of about 15,000 asteroidal, cometary, and trans-Neptunian dust particles under the gravitational influence of planets (excluding Pluto for asteroidal and cometary particles), the Poynting-Robertson drag, radiation pressure, and solar wind drag. Results of some of these

integrations were presented by Ipatov et al. (2004) and Ipatov & Mather (2006a-b). As in Liou et al. (1999) and Moro-Martin & Malhotra (2002), we assume the ratio of solar wind drag to Poynting–Robertson drag to be 0.35. In this section we describe the model used for our studies of the migration of dust particles.

In our runs for asteroidal and cometary particles, the values of β , the ratio of the sun’s radiation pressure force to gravitational force, varied from ≤ 0.0004 to 0.4. Burns et al. (1979) obtained $\beta = 0.573 Q_{pr} / (\rho s)$, where ρ is the particle’s density in grams per cubic centimeter, s is its radius in micrometers, and Q_{pr} is the radiation pressure coefficient, which is close to unity for particles larger than 1 μm . For silicates at density of 2.5 g/cm^3 , the β values 0.004, 0.01, 0.05, 0.1, and 0.4 correspond to particle diameters d of about 120, 47, 9.4, 4.7, and 1 microns, respectively. For water ice, d is greater by a factor of 2.5 than that for silicate particles. The orbital evolution of dust particles was studied for a wider range of masses (including particles up to several millimeters) of asteroidal and cometary particles than in the papers by other authors (e.g., Dermott et al. 2001, 2002; Gorkavyy et al. 2000; Grogan et al. 2001; Kortenkamp & Dermott 1998; Liou et al. 1995, 1996, 1999; Liou & Zook 1999; Moro-Martin & Malhotra 2002, 2003; Ozernoy 2001; Reach et al. 1997). Smaller particles have a larger surface per unit of mass of particles. It has been proposed (Grün et al. 1985) that the main contribution to the zodiacal light is from particles that range from 20 to 200 μm in diameter (for silicate particles, this range corresponds to β about 0.002–0.02). According to Grün et al. (2000), the Lorentz force is comparable to solar gravitational interaction for particles of $d \sim 0.1 \mu\text{m}$ at 1 AU and of $d \sim 1 \mu\text{m}$ at 50 AU. Interstellar particles dominate among such small particles, and are not believed to be significant contributors to the zodiacal light. We considered mainly larger interplanetary particles, so we did not include the Lorentz force in our runs.

Migration of dust particles was integrated using the Bulirsh-Stoer method (BULSTO) with the relative error per integration step less than 10^{-8} . The SWIFT integration package by Levison & Duncan (1994) was modified to include the additional forces of radiation pressure, Poynting–Robertson drag, and solar wind drag. The integration continued until all of the particles either collided with the sun or reached 2000 AU from the sun. For small β , lifetimes exceeded 50–80 Myr (240 Myr for trans-Neptunian particles). In each run (with a fixed source of particles and $\beta = \text{const}$) we took $N \leq 250$ particles, because for $N \geq 500$ the computer time per calculation for one particle was several times greater than for $N = 250$. The total number of particles in several tens of runs (with different β and different sources of particles) was about 15,000. In our runs, orbital elements were stored with a step of d_t of 20 yr for asteroidal and cometary particles and 100 yr for trans-Neptunian particles during all considered time intervals. The stored orbital elements of all particles during their dynamical lifetimes were then used in our studies of the velocities of particles presented in the next

section.

The planets were assumed to be material points. However, using orbital elements obtained with a step d_t , Ipatov and Mather (2006a) calculated the mean probability of a collision of a particle with the planet during the particle lifetime. The total probability of collisions of all particles with planets in one run is small. Therefore, in most runs the results obtained will be exactly the same whether or not we consider collisions of particles with planets during integration. Even if there were a particle that actually collides with a planet, the sum of dynamical lifetimes of all particles and the distribution of particles over their orbital elements during their dynamical lifetimes will be practically the same as in the model for which planets are considered as material points. Destruction of particles due to their collisions with other particles is also not considered in the present paper. The destruction affects mainly lifetimes of particles and their size distributions at different distances from the sun, but not the distribution of the particles orbital elements during their migration in the zodiacal cloud. In future models, which will consider the size distributions of particles, we plan to take into account the destruction of particles.

The initial positions and velocities of asteroidal particles used in our models were the same as those of the first N numbered main-belt asteroids (JDT 2452500.5), i.e., dust particles are assumed to leave the asteroids with zero relative velocity. The initial positions and velocities of the trans-Neptunian particles were the same as those of the first trans-Neptunian objects (JDT 2452600.5). The initial positions and velocities of cometary particles were the same as those of Comet 2P/Encke ($a_o \approx 2.2$ AU, $e_o \approx 0.85$, $i_o \approx 12^\circ$), or Comet 10P/Tempel 2 ($a_o \approx 3.1$ AU, $e_o \approx 0.526$, $i_o \approx 12^\circ$), or Comet 39P/Oterma ($a_o \approx 7.25$ AU, $e_o \approx 0.246$, $i_o \approx 2^\circ$), or long-period comets ($e_o = 0.995$, $q_o = a_o \cdot (1 - e_o) = 0.9$ AU or $q_o = 0.1$ AU, i_o varied from 0 to 180° in each run, particles started at perihelion; these runs are denoted as lp runs). We considered Encke particles starting near perihelion (runs denoted as 2P), near aphelion (runs denoted as ‘2P 0.5t’), and when the comet had orbited for $P_a/4$ after perihelion passage, where P_a is the period of the comet (runs denoted as ‘2P 0.25t’). Note that semimajor axes and eccentricities of dust particles differed from those of parent bodies, but inclinations were the same.

For cometary particles, the initial value of time τ when perihelion was passed was varied for different particles with a step $d\tau = 1$ day or $d\tau = 0.1$ day near the actual value of τ for the comet. Comet 10P is an example of a typical Jupiter-family comet moving inside Jupiter’s orbit; Comet 39P moves outside Jupiter’s orbit. Comet 2P is the only known high-eccentricity comet with aphelion distance $Q < 4.2$ AU. It comes close to the sun and produces a lot of dust. Our initial data for dust particles are different from those in previous papers, and the parent comets producing dust are different (exclusive of Comet 2P) from

those considered earlier.

3. Model Used for Calculation of the Scattered Line Profile

We calculated how the solar spectrum was changed after the light was scattered by the dust particles and observed at earth. This was carried out by first considering all orbital elements of dust particles during a single run, which were stored in computer memory with a step $d\tau$ (see the previous section). Based on these stored orbital elements, we calculated velocities and positions of particles and the earth during the dynamical lifetimes of the particles. For each pair of positions of a particle and the earth, we then calculated many ($\sim 10^2$ - 10^4 , depending on a run) different positions of the particle and the earth during the period P_{rev} of revolution of the particle around the sun, assuming that orbital elements do not vary during P_{rev} . This number is smaller for runs with larger maximum dynamical lifetimes of particles.

The model, which is based on all positions and velocities of dust particles during their dynamical lifetimes, represents the zodiacal cloud for the case when small bodies continuously produce dust at a constant rate along their orbits; seasonal effects and jumps in production of dust are not considered in this model. The model allows one to study the principal differences between spectra corresponding to particles produced by asteroids, comets, and trans-Neptunian objects. More complicated models to study the fractions of particles of different origin can be considered in the future.

The choice of a scattering function was based on analyses of dependences of scattering functions on angles θ and ϵ (see below) and wavelength presented in several papers (e.g., Giese 1963; Giese & Dziembowski 1969; Leinert 1975; Leinert et al. 1976; Weiss-Wrana 1983; Hong 1985; Lamy & Perrin 1986), which mainly followed the Mie theory for scattering. The scattering function depends on the composition of particles, their sizes, and other factors. However, we considered three simple scattering functions: (1) $g \propto 1/\theta$ for $\theta < c$, and $g \propto 1+(\theta - c)^2$ for $\theta > c$, where θ is the angle between the earth and the sun, as viewed from the particle in radians and $c = 2\pi/3$ radian; (2) g having the same functional form as above, but with θ replaced by elongation ϵ , the angle between the particle and the sun, as viewed from the earth (eastward from the sun); (3) isotropic scattering. For all three functions, the intensity I of light that reaches the earth was considered to be proportional to $\lambda^2 \cdot (R * r)^{-2}$, where r is the distance between the particle and the earth, R is the distance between the particle and the sun, and λ is the wavelength of light. Since we considered the scattering near a single spectral line, wavelength λ in our runs was essentially a constant. Except for lines of sight close to the sun, these three scattering functions give virtually the same results (see

below). Since the differences between the functions that we considered were much greater than the differences between scattering functions presented in the publications cited above, we conclude that we need not worry about the precise form of the scattering.

For each particle position, we calculated the velocity relative to the sun, the velocity relative to the earth, and its respective distance to the earth and to the sun, r and R . These parameters and the scattering function were then used to construct the solar spectrum received at the earth after light had been scattered by all the particles located within some limited solid angle (beam) along a line of sight from the earth. The direction of the beam is characterized by its eastern elongation from the sun ϵ , and by its inclination above the ecliptic plane. Particles in beams of diameter 2° (Fig. 1) and 2.5° (other figures) were considered. Projections of relative velocities of particles on the lines of sight from the earth and the sun to particles were used for analysis of the Doppler shift. In each run, particles all had the same size, the same β , and the same source (e.g., asteroidal).

4. Variations in Solar Spectrum Caused by Scattering by Dust Particles

4.1. Centroid velocity shifts

Figure 1 shows sample spectra of scattered Mg I $\lambda 5184$ obtained from these calculations toward sightlines in the antisolar direction (Fig. 1a,c) and toward the ecliptic pole (Fig. 1b,d). The spectra consist of intensity vs. wavelength shift $\Delta\lambda$ with respect to 5183.62 Angstrom. The thinnest line in Figure 1 denotes the initial (unscattered) solar spectrum. For asteroidal ('ast') and Comet Encke ('2P') particles, the solar spectrum received at the earth is found to be nearly independent of the scattering function, while for trans-Neptunian ('tn') particles, the results for scattering function (3), denoted as 'tn3', differ slightly from (1) and (2), denoted as 'tn 1' and 'tn 2', respectively. In the legend in the figure, the first number (0.2 in Fig. 1a,c) denotes β , and the next number in Figures 1a,c denotes elongation ϵ (in degrees). The WHAM observations are also presented for comparison. These observations and all other plots in Figure 1c,d were stretched so that the minimum in the line was at approximately the same depth as that for the initial solar spectrum. The continuum levels were also set to be the same (equal to 1) for all plots. Similar plots at $\epsilon=90^\circ$ and $\epsilon=270^\circ$ for zero inclination above the ecliptic plane were presented by Ipatov et al. (2005). Unlike results by Clarke et al. (1996) who considered spectrum near 4861 Angstrom (H_β line of hydrogen), our modeled spectra don't exhibit strong asymmetry. We similarly found that minima in the plots of dependencies of the intensity of light on its wavelength near 5184 Angstrom are not as deep as those for the initial solar spectrum. Note that the value of ϵ in the paper by Clarke et al. (1996) is measured in the opposite clockwise direction than in

our present paper, so our 90° corresponds to 270° in their paper.

At the North Ecliptic Pole, the calculated spectrum was shifted slightly to the left relative to the solar spectrum for asteroidal particles and slightly to the right (to the red) for particles originating from Comet 2P (Fig. 1b,d). These shifts may be due to small asymmetries in the model particle distributions with respect to the ecliptic plane. The spectra of 10P and 39P particles and those from long-period comets were very similar to each other. For cometary particles, the line profile has a flatter bottom than that for asteroidal particles, but it was not so wide as the observed spectrum presented in (Reynolds et al. 2004). None of our model runs matched the large width of the observation toward the ecliptic pole. This issue will not be addressed in this paper, but will be a topic for future investigation.

The calculated model spectra along the ecliptic plane are in general agreement with the observations. For different values of ϵ , based on the model spectra, which use the distribution of velocities and positions of dust particles in our run, we determined the Doppler shift of the scattered Mg I line with respect to the centroid wavelength of the unscattered solar profile. The plot of this characteristic velocity vs. the solar elongation ϵ along the ecliptic plane is called the ‘velocity-elongation’ plot. For ‘velocity-elongation’ plots marked by c , we considered the shift of the centroid (the ‘center of mass’ of the line), while ‘velocity-elongation’ plots marked by m denote the shift of the minimum of the line. ‘Velocity-elongation’ plots for different scattering functions are denoted as $c1$ and $m1$ for the scattering function 1, as $c2$ and $m2$ for the function 2, and as $c3$ and $m3$ for the function 3. The lines in Figure 1 are nearly symmetric, so the results for ‘ c ’ and ‘ m ’ in Figure 2 differ only a little. Brief discussions of ‘velocity-elongation’ plots obtained in our runs with observations have been made by Ipatov et al. (2005, 2006), Madsen et al. (2006), and Ipatov and Mather (2006a). Below we compare the ‘velocity-elongation’ plots in more details.

The details of the model spectra depend on ϵ , β , i_o , and the source of particles. Different particles populations produce clearly distinct model spectra of the zodiacal light. The ‘velocity-elongation’ plots obtained for different scattering functions were similar at $30^\circ < \epsilon < 330^\circ$ (Fig. 2); though the difference was greater for directions close to the sun. Some jumps in the plots are caused by small number statistics for these runs. In Figures 3-8 the results were obtained using only the second scattering function.

A comparison of the observed ‘velocity-elongation’ plot with those obtained from our model for dust particles of different sizes (i.e., different values of β) produced by asteroids, comets (2P/Encke, 10P/Tempel 2, 39P/Oterma, long-period), and trans-Neptunian objects allowed us to draw some conclusions about the sources of zodiacal dust particles. Asteroidal, trans-Neptunian, and 2P particles populations produce clearly distinct model spectra of the

zodiacal light. The differences between ‘velocity-elongation’ plots for several sources of dust reached its maximum at ϵ between 90° and 120° (Figs. 3–6). For future observations of velocity shifts in of the zodiacal spectrum, it will be important to pay particular attention to these elongations.

We consider the amplitude of ‘velocity-elongation’ curves as $v_a=(v_{\max}-v_{\min})/2$, where v_{\min} and v_{\max} are the minimum and maximum values of velocities at $90^\circ<\epsilon<270^\circ$. The observational value of v_a is about 12 km/s (if we smooth the plot). For several dust sources, the characteristic values of v_a , v_{\min} , and v_{\max} are presented in Table 1. Mean eccentricities e_z and mean inclinations i_z at distance from the sun $1\leq R\leq 3$ AU are also included in the table. For asteroidal dust, the ‘velocity-elongation’ plots had lower amplitudes than the observations (Fig. 3a–b). The plots obtained at different β differed little from each other, especially at $\beta<0.01$. For 10P particles, the ‘velocity-elongation’ amplitudes were also lower than that of the observations (Fig. 3c–d). The difference between the plots obtained for 10P particles at different β was greater than that for asteroidal particles, but was usually less than that for other sources of particles considered. On the other hand, the ‘velocity-elongation’ curve corresponding to particles produced by Comet 2P have slightly larger amplitudes than the observed curve (Fig. 4a-b). So perhaps a combination of cometary 2P dust particles and asteroidal particles could provide a result that is close to the observational ‘velocity-elongation’ curve. The velocity amplitudes v_a for particles originating from long-period comets are much greater than those for the observational curve (Fig. 6b).

The orbit of Comet 39P is located outside Jupiter’s orbit. Studies of the migration of 39P particles thus give some information about the the migration of particles originating beyond Neptune’s orbit that have reached the orbit of Jupiter. For 39P particles and $0.01\leq\beta\leq 0.2$ at $60^\circ<\epsilon<150^\circ$, ‘velocity-elongation’ amplitudes were smaller than those for the observations (Fig. 5a), while for $\beta\leq 0.004$, the curves more closely match the observations (Fig. 5b). For such small β , only a small number of particles entered inside Jupiter’s orbit, and statistics were poor. The distribution of particles over their orbital elements could be somewhat different if we had considered a greater number N of particles in one run, but the difference between the curves obtained at different N will not be more than the difference between the curves obtained at adjacent values of β presented in the figure. At $\beta=0.0001$, particles spent on average more time in the zodiacal cloud than for other runs, but it was due mainly only to one particle, which during about 9 Myr moved inside Jupiter’s orbit before its collision with the sun. In reality such a particle could sublimate or be destroyed in collisions during its dynamical lifetime. Small number statistics may also be responsible for the spread of results for the trans-Neptunian dust in Figure 6a. If there had been a greater number of particles in the runs, the differences between the corresponding plots would probably have been smaller. There was a zero vertical shift for the observational plot. Plots for asteroidal,

10P, and 39P particles are shifted a little down, and that for 2P particles was shifted up relative to the observational plot. So a combination of different sources of particles could give a zero vertical shift.

For trans-Neptunian dust particles, velocity amplitudes v_a were greater than the observational values at $\beta \geq 0.05$ and were about the same at $\beta = 0.01$ (Fig. 6a). So together with cometary particles, trans-Neptunian particles can compensate small values of v_a for asteroidal particles. The difference between different plots in Fig. 6a may be caused partly by small statistics, as only a few trans-Neptunian particles in each run (at fixed β) entered inside Jupiter's orbit. The observational plot was mainly inside the region covered by trans-Neptunian plots obtained for different β , but at $180^\circ < \epsilon < 270^\circ$ it was mainly above the trans-Neptunian curves.

In the future we plan to explore the fractions of particles of different origin in the overall dust population based on various observations and taking into account a model for the size distribution of particles. Here we present estimates based on a much simpler, two-component zodiacal dust cloud that fits the observations. For example, with a velocity amplitude $v_a = 9$ km/s for asteroidal dust and at $v_a = 14$ km/s for 2P particles, the fraction f_{ast} of asteroidal dust would need to be 40%. If all of the cometary particles in the zodiacal dust were from long-period comets ($v_a = 33$ km/s), then $f_{ast} = 88\%$. The contribution of lp particles to the zodiacal light can not be large also because their inclinations are large and IRAS observations showed (Liou et al. 1995) that most of the zodiacal light is due to particles with inclinations $i < 30^\circ$. At $\beta \geq 0.004$, lp particles are quickly ejected from the solar system, so among zodiacal dust we can find only lp particles greater than $100 \mu\text{m}$. The contribution of lp particles to the total mass of the zodiacal cloud is greater than their contribution to the brightness I , as a surface of a particle of radius r_p is proportional to r_p^2 , and its mass M is proportional to r_p^3 (i.e., $M/I \propto r_p$). Dynamical lifetimes of lp particles at $\beta \leq 0.002$ (i.e., at diameters greater than $200 \mu\text{m}$) can exceed several Myrs (i.e., exceed mean lifetimes of asteroidal and 2P particles), so the fraction of lp particles in the zodiacal cloud can be greater than their fraction in the new particles that were produced by small bodies or came from other regions of the solar system. Dynamical lifetimes of dust particles are greater for smaller r_p (Ipatov and Mather 2006a), and some particles can be destroyed in collisions with other particles. So the mass distributions of particles produced by small bodies are different from the mass distributions of particles located at different distances from the sun.

A significant fraction of cometary dust in the near-earth space was proposed by Liou et al. (1995) and Zook (2001). Liou et al. (1995) based his estimates of the fraction of cometary dust (3/4 to 2/3) on comparison of the migration of $9 \mu\text{m}$ diameter dust particles that produced by comet Encke-type parent bodies with the IRAS observations of the shape

of the zodiacal cloud. Based on cratering rates from an ensemble of earth- and lunar-orbiting satellites, Zook (2001) estimated that the cometary contribution to the near-earth flux of particles is $\sim 75\%$. Ozernoy (2001) compared the computer simulation results of migration of $1\ \mu\text{m}$ and $5\ \mu\text{m}$ dust particles with the COBE/DIRBE data and showed that the trans-Neptunian dust contributes as much as $\sim 1/3$ of the total number density near the earth. Grogan et al. (2001) suggested that at least 30% of zodiacal dust comes from the break-up of asteroids in order to explain formation of dust bands. The conclusions on a considerable fraction of cometary dust are also in agreement with earlier studies of the dynamics of Jupiter-family comets (Ipatov & Mather 2003, 2004a-b, 2006a), which showed that some former cometary objects could get high eccentric orbits located entirely inside Jupiter’s orbit and move in such orbits for a long time. Some of these objects could disintegrate producing a substantial amount of dust. Comparison of the number density of migrating dust particles with the observation that number density is constant at 3-18 AU from the sun (Ozernoy 2001, Landgraf 2002, Ipatov & Mather 2005, 2006a) is also consistent with that a fraction of cometary dust particles is significant (perhaps dominant) inside Saturn’s orbit.

4.2. Line widths

Observations by Reynolds et al. (2004) also provided the FWHM (full width at half maximum) of the Mg I line in the zodiacal light. In Figure 7, their values are marked by crosses. Most of the observed values were between 70 and 80 km/s, with a mean value of 76.6. In Figure 7, we compare these observations with the FWHM values obtained from our model line profiles. The values are different for different β and different sources of the dust. For particles started from asteroids, comets 2P, 10P and 39P, and long-period comets, the mean (at $30^\circ < \epsilon < 330^\circ$) values of FWHM are about 74, 81-88, 76-77, 76-77, 73-86 km/s, respectively. For 2P particles, the values of FWHM depend on β and the place of origin from the orbit. The mean values of FWHM obtained for particles started from long-period comets can differ considerably in different runs with different β . Discrete values of the width in Figure 7 are caused by a discrete model of spectra. As observational values of the width can differ by 10 km/s for close values of ϵ , there is no need to calculate accurately the width in our models.

At $\beta \leq 0.004$ for particles started from Comet 2P, the width is greater at $\epsilon \approx 220^\circ$ than at $\epsilon \approx 45^\circ$ (Fig. 7b-d). For other sources of dust, the width is approximately independent of ϵ at $30^\circ < \epsilon < 330^\circ$. The widths all become relatively large at $-15^\circ < \epsilon < 15^\circ$, where there are no observations. At $\beta \geq 0.1$ for particles started from Comet 2P, the widths are generally narrower than that at smaller β . For asteroidal particles, on the contrary, the width is

maximum at $\beta=0.4$. For 10P and 39P particles, the mean width is slightly greater for smaller β at $0.0001 \leq \beta \leq 0.1$ (Fig. 8). For particles started from long-period comets (at $e_z=0.995$, $q=a(1-e)=0.9$ AU, and orbital inclinations distributed between 0 and 180°) the mean width usually is even less than that for 2P particles at the same β .

As it is summarized in Figure 8, the FWHM for asteroidal dust is significantly less than the 77 km/s FWHM of the observations. To fit the observations, we need to consider a significant fraction of cometary particles. 2P particles and particles started from long-period comets provided large values of the width in most runs, but the width varied considerably in such runs depending on β and the place of start (i.e., the value of true anomaly) from the comet.

5. Orbital Elements of Zodiacal Particles

In order to understand the variations in the model line profiles with the source and size of particles, we examined the values of mean eccentricities and mean orbital inclinations of particles at different distances R from the sun (Figs. 9-12). These data show that, in general, the velocity amplitudes of the Mg I line are greater for greater mean eccentricities and inclinations, but they depend also on distributions of particles over their orbital elements.

The main contribution to the brightness of a dust cloud observed at the earth is from particles located at $R < 3$ AU. Therefore, because only positions of particles at $R \geq 1$ AU are used for calculation of the brightness of particles at $90^\circ \leq \epsilon \leq 270^\circ$, if it is not mentioned specially, the mean eccentricities e_z and orbital inclinations i_z refer to $1 \leq R \leq 3$ AU. At $\epsilon=270^\circ$ prograde particles move in the same direction as the earth, but usually slower because they are located farther from the sun than the earth. Therefore, velocities of Mg I line are usually positive at $\epsilon=90^\circ$ and negative at $\epsilon=270^\circ$.

The values of e_z , i_z , v_a , v_{\min} , and v_{\max} for particles from different sources are presented in Table 1 for several values of β . This table and Figures 3-6, 9-12 show that at $e_z < 0.5$ (e.g., for particles started from asteroids and Comet 10P) the velocity amplitudes v_a are usually smaller than the observed amplitude (12 km/s), while for some runs at $e_z > 0.5$ (e.g., for runs 2P and lp), v_a is greater than the observed amplitude. Thus the WHAM observations correspond to a mean orbital eccentricity e_z of about 0.5. However, the velocity amplitudes of the line depend not only on e_z , but also on the distribution of all orbital elements of dust particles. For example, for trans-Neptunian particles at $0.05 \leq \beta \leq 0.4$, we have relatively large amplitudes ($v_a \approx 16$ km/s), even though $e_z < 0.5$; the values of i_z in this case were a little greater than for other sources of particles at $e_z < 0.5$. Also, for trans-Neptunian particles, the

values of v_a were smaller at $\beta=0.01$ than at $0.05 \leq \beta \leq 0.4$, though e_z was greater at $\beta=0.01$.

The velocity amplitudes also depend on inclinations, because high inclination orbits have smaller projections of their orbital velocities on the lines of sight from the earth and the sun to particles near the ecliptic plane. For particles originating from long-period comets (lp particles), the values of v_a are significantly greater than those for dust particles from other sources, and the values of i_z ($>105^\circ$) were much greater than for other runs. For lp runs at $\beta=0.002$ and $q=0.9$ AU, e_z was smaller (<0.25) than in most other runs, but v_a was large (41 km/s), because i_z was large ($154\text{--}160^\circ$). Note that mean initial inclinations for lp runs were about 90° (initial orbital inclinations were distributed uniformly between 0 and 180°), but the mean inclinations of migrating particles were greater than 90° (see Fig. 12d).

The velocities of Mg I line depend not only on mean eccentricities and inclinations of particles, but also on the distributions of the orbital elements. The distribution of orbital parameters and the resulting scattered line profile is dependent upon β , because β influences the lifetime of the particle. Dynamical lifetimes of particles are greater for smaller β . In the case of particles started from Comet 2P, for runs presented in Figures 13a,c,d, the maximum lifetimes were less than 5 Kyr, and for runs presented in Fig. 13b,f they were about 50-60 Kyr. Particles that migrate more slowly into the sun (smaller β) interact with planets for a longer time, and therefore they exhibit a wider range of parameter values, even though they have the same origin. This explains the difference between the plots in Figure 13 obtained at different β (wider range of e was obtained at smaller β). As the motion is stochastic and the number of particles in our runs is not large, there may be no strict dependence on β . The plots of the velocities of MgI line for ‘2P 0.25t’ and ‘2P 0.5t’ runs presented in Fig. 4c-d are higher than the observational line at large β . In this case, all eccentricities are large at $a > 1$ AU (Fig. 13a,c,d), lifetimes of all particles are close to each other and are very short (<5 Kyr), and all particles moved practically in the same way. For $\beta=0.05$, the maximum lifetime of 2P-particles started at aphelion (‘2P 0.5t’ run) was greater by a factor of 4 than that for ‘2P 0.25t’ run. Therefore for $\beta=0.05$, variations in e at the same a were greater for ‘2P 0.5t’ run than for ‘2P 0.25t’ run. For many particles other than 2P particles, lifetimes are several tens or several hundreds of thousands of years and can reach tens of millions of years (Ipatov and Mather 2006a). Besides, more particles start from Comet 2P in its perihelion (in this case, the plots do not differ much from the observational plot even at large β) than in aphelion. Therefore the zodiacal light contribution is very small for particles with $\beta \geq 0.05$ started from Comet 2P at aphelion or in the middle of the orbit.

Finally, we examine the number density $n(R)$ of particles with distance R from the sun. In Figures 14a-c we present the values of α in $n(R) \propto R^{-\alpha}$ for R equal to 0.3 and 1 AU (a), at $R=0.8$ and $R=1.2$ AU (b), and at R equal to 1 and 3 AU (c). These results can

then be compared to values of α deduced from observations of the actual zodiacal cloud. The micrometeoroid flux (10^{-12} g - 10^{-9} g, i.e., at $d < 5 \mu\text{m}$ for $\rho = 2.5 \text{ g/cm}^3$, or at $\beta \geq 0.1$) measured on board Helios 1 during 1975 is compatible with a number density $n(R) \propto R^{-1.3}$ at distance R from the sun between 0.3 and 1 AU (Grün et al. 1977, Leinert et al. 1981). Pioneer 10 observations between the earth's orbit and the asteroid belt yielded $n(R) \propto R^{-1.5}$ for particles of mass $\sim 10^{-9}$ g (Reach 1992).

Note that in our models, at $0.3 \leq R \leq 1$ AU and $0.001 \leq \beta \leq 0.2$ all values of α exceed 1.9 for 2P-particles and are smaller than 1.1 for asteroidal particles (Fig. 14a). At $\beta \geq 0.005$, the values of α for particles started from other considered comets were less than 1.5, but were mainly greater than those for asteroidal particles. We can get $\alpha = 1.3$ for two component dust cloud if we consider 86% of particles with $\alpha = 1.1$ and 14% of particles with $\alpha = 2$. So the fraction of 2P particles needed to fit the Helios observations can be less than 15%. At $\beta \geq 0.1$ and $0.8 \leq R \leq 1.2$ AU, the mean value of α for all points in Figure 14b was a little smaller than 1.5. For cometary dust, α was mainly greater than for asteroidal dust; this difference was greater at $\beta \leq 0.05$ than for $\beta \geq 0.1$. At $\beta \leq 0.2$, the values of α for 2P-particles were greater than for other sources of dust. At $1 \leq R \leq 3$ AU for most of the dust sources, the values of α were mainly greater than 1.5 (Fig. 14c). For $0.1 \leq \beta \leq 0.2$, the values of α for particles started from trans-Neptunian objects and Comet 39P better fit the observational value of 1.5 than those for particles from other sources (including asteroidal dust). So our studies of the distributions of particles over R and of the velocities of Mg I line testify that a fraction of trans-Neptunian particles among zodiacal dust particles can be considerable.

6. Conclusions

Our study of velocities and widths of the scattered Mg I line in the zodiacal light is based on the distributions of positions and velocities of migrating dust particles originating from various solar system sources. These distributions were obtained from our integrations of the orbital evolution of particles started from asteroids, comets, and trans-Neptunian objects. A comparison of our models with the observations of velocities and widths of the zodiacal Mg I line made by Reynolds et al. (2004) shows that asteroidal dust particles alone cannot explain these observations, and that particles produced by comets, including high-eccentricity comets (such as Comet 2P/Encke and long-period comets), are needed. A considerable fraction of trans-Neptunian dust particles among zodiacal dust particles also fits different observations. The mean eccentricity of zodiacal dust particles that best fit the WHAM observations is estimated to be about 0.5.

Acknowledgements

This work was supported by NASA (NAG5-12265) and by the National Science Foundation through AST-0204973.

REFERENCES

- Burns, J. A., Lamy, P. L., & Soter, S. 1979, *Icarus*, 40, 1
- Clarke, D., Matthews, S. A., Mundell, C. G., & Weir, A. S. 1996, *A&A*, 308, 273
- Dermott, S. F., Grogan, K., Durda, D. D., et al. 2001, in *Interplanetary dust*, ed. B. A. S. Gustafson, S. Dermott, & H. Fechtig (Berlin: Springer-Verlag), 569
- Dermott, S. F., Durda, D. D., Grogan, K., & Kehoe, T. J. J. 2002, in *Asteroids III*, ed. W. F. Bottke, Jr., A. Cellino, P. Paolicchi, & R. P. Binzel (Tucson: The University of Arizona Press), 423
- East, I. R., & Reay, N. K. 1984, *A&A*, 139, 512
- Fried, J. M. 1978, *A&A*, 68, 259
- Giese, R. H. 1963, *Space Sci. Rev.*, 1, 589
- Giese, R. H., & v. Dziembowski, C. 1969, *Space Sci. Rev.*, 17, 949
- Gorkavyi, N. N., Ozernoy, L. M., Taidakova, T., & Mather, J. C. 2000, *astro-ph/0006435*
- Grogan, K., Dermott, S. F., & Durda, D. D. 2001, *Icarus*, 152, 251
- Grün, E., Fechtig, H., Kissel, J., & Gammelín, P. 1977, *J. Geophys.*, 42, 717
- Grün, E., Zook, H.A., Fechtig, H., & Giese, R.H. 1985, *Icarus*, 62, 244
- Grün, E., Kruger, H., & Landgraf, M. 2000, in *Proc. ESO workshop (Nov. 2-5, 1998, Garching, Germany)*. Springer, 99
- Hicks, T. R., May, B. H., & Reay, N. K. 1974, *MNRAS*, 166, 439
- Hong, S. S., 1985, *A&A*, 146, 67
- Ipatov, S. I., & Mather, J. C. 2003, *Earth, Moon, & Planets*, 92, 89
- Ipatov, S. I., & Mather, J. C. 2004a, in *Annals of the New York Acad. of Sci.*, v. 1017, *Astrodynamics, Space Missions, and Chaos*, ed. B. Belbruno, D. Folta, & P. Gurfil (New York: NYAS), 46
- Ipatov, S. I., & Mather, J. C. 2004b, *Adv. Space Res.*, 33, 1524
- Ipatov, S. I. & Mather, J. C. 2006a, *Adv. Space Res.*, 37, 126

- Ipatov, S. I., & Mather, J. C. 2006b, in *Dust in Planetary System*, ed. H. Kruger & A. Graps (ESA), in press
- Ipatov, S. I., Mather, J. C., & Taylor, P. A. 2004, in *Annals of the New York Acad. of Sci.*, v. 1017, *Astrodynamics, Space Missions, and Chaos*, ed. B. Belbruno, D. Folta, & P. Gurfil (New York: NYAS), 66
- Ipatov, S. I., Kutyrev, A. S., Madsen, G. J., Mather, J. C., Moseley, S. H., & Reynolds, R.J. 2005, *Lunar Planet. Sci. Conf.*, 36, 1266.
- Ipatov, S. I., Kutyrev, A. S., Madsen, G. J., Mather, J. C., Moseley, S. H., & Reynolds, R.J. 2006, *Lunar Planet. Sci. Conf.*, 37, 1471.
- James, J. F. 1969, *MNRAS*, 142, 45
- Kortenkamp, S. J. & Dermott., S. F. 1998, *Icarus*, 135, 469
- Landgraf, M., Liou, J.-C., Zook, H. A., & Grün, E. 2002, *AJ*, 123, 2857
- Lamy, P. L. & Perrin, J.-M. 1986, *A&A*, 163, 269
- Levison, H.F. & Duncan, M.J. 1994, *Icarus*, 108, 18
- Leinert, C. 1975, *Space Sci. Rev.*, 18, 281
- Leinert, C., Link, H., Pitz, E., & Giese, R. H. 1976, *A&A*, 47, 221
- Leinert, C., Richter, I., Pitz, E., & Plank, B. 1981, *A&A*, 103, 177
- Liou, J.-C. & Zook, H. A. 1999, *AJ*, 118, 580
- Liou, J.-C., Dermott, S. F., & Xu, Y. L. 1995, *Planet. Space Sci.*, 43, 717
- Liou, J.-C., Zook, H. A., & Dermott, S. F. 1996, *Icarus*, 124, 429
- Liou, J.-C., Zook, H. A., & Jackson, A. A. 1999, *Icarus*, 141, 13
- Madsen, G. J., Reynolds, R. J., Ipatov, S. I., Kutyrev, A. S., Mather, J. C., & Moseley, S. H. 2006, in *Dust in Planetary System*, ed. H. Kruger & A. Graps, (ESA), in press
- Moro-Martin, A. & Malhotra, R. 2002, *AJ*, 124, 2305
- Moro-Martin, A. & Malhotra, R. 2003, *AJ*, 125, 2255
- Ozernoy, L. M. 2001, in *IAU Colloq. 204: The Extragalactic Infrared Background and its Cosmological Implications*, ed. M. Harwit & M. G. Hauser, 17, astro-ph/0012033

Reach, W.T. 1992, ApJ, 392, 289

Reach, W. T., Franz, B. A., & Weiland, J. L. 1997, Icarus, 127, 461

Reynolds, R. J., Madsen, G. J., & Moseley, S. H. 2004, ApJ, 612, 1206

Weiss-Wrana, K. 1983, A&A, 126, 240

Zook, H. A. 2001, in Accretion of extraterrestrial matter throughout Earth's history, ed. B. Peucker-Ehrenbrink and B. Schmitz (NY: Kluwer), 75

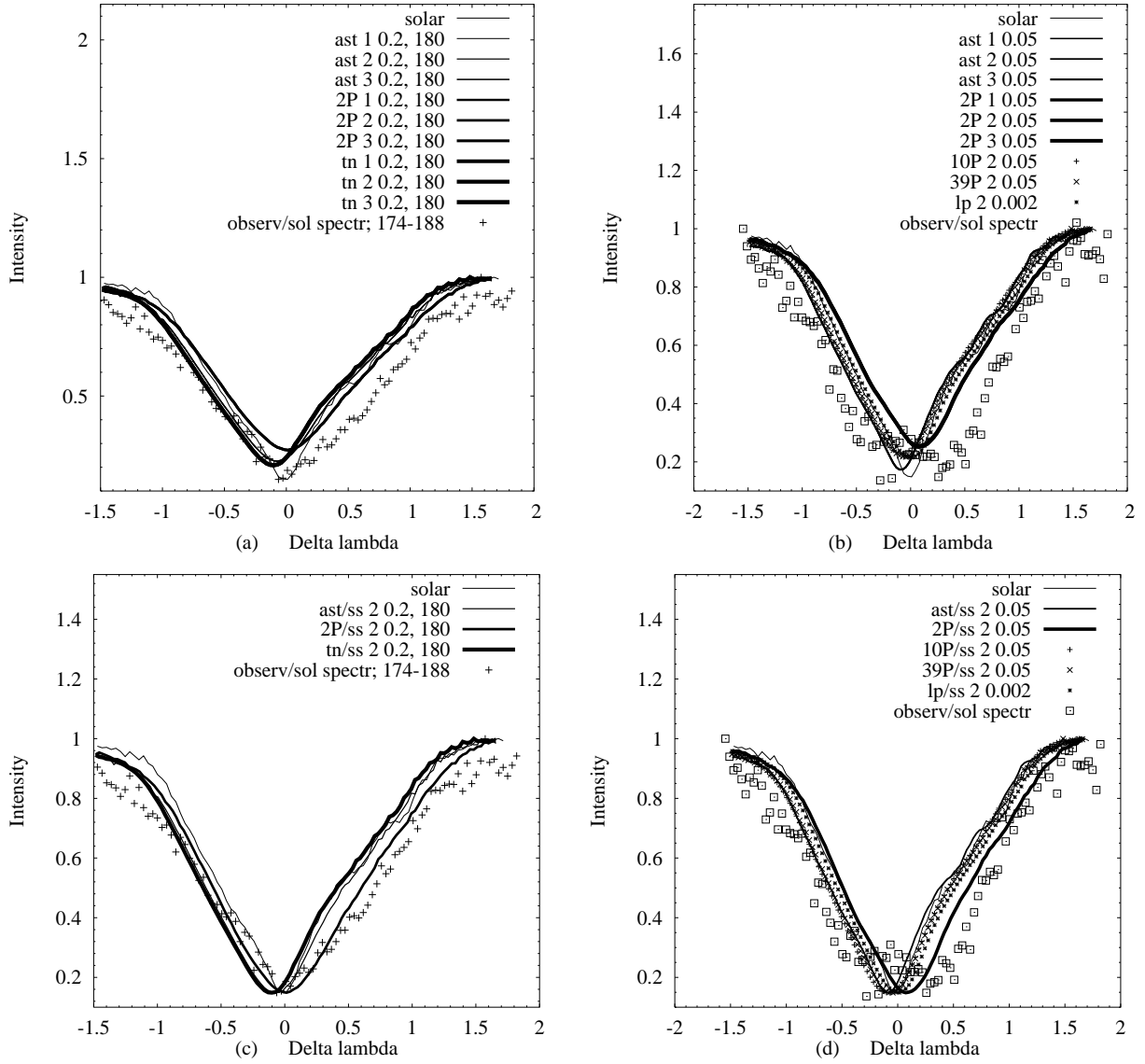


Fig. 1.— Dependence of the intensity of light vs. its wavelength λ (in Angstrom) at $\beta=0.2$, $\epsilon=180^\circ$, in the ecliptic plane (a,c) and at $\beta=0.05$ (exclusive for lp particles considered at $\beta=0.002$) toward the north ecliptic pole (b,d). Zero of $\Delta\lambda=\lambda-\lambda_o$ corresponds to $\lambda=\lambda_o=5183.62$ Angstrom. The plots for dust particles started from asteroids, trans-Neptunian objects, Comet 2P at perihelion, comets 10P and 39P are denoted by ‘ast’, ‘tn’, ‘2P’, ‘10P’, and ‘39P’, respectively. Data for particles started from long-period comets (lp) at $e_o=0.995$, $q_o=0.9$ AU, and i_o distributed between 0 and 180° , are marked as ‘lp’. The curves marked by ‘ast 1’, ‘tn 1’, and ‘2P 1’ are for scattering function 1, ‘ast 2’, ‘tn 2’, and ‘2P 2’ are for function 2, and ‘ast3’, ‘tn3’, and ‘2P 3’ are for function 3. The curves are practically the same for all three functions. Marks in Fig. (a,c) are for average intensity for observations at $174^\circ \leq \epsilon \leq 188^\circ$, and marks in Fig. (b,d) are for average observations toward the north ecliptic pole. Coordinates of marks for ‘observ/sol spectr’ were obtained from observational data by making it have the same minimum value as the solar spectrum. In Fig. (c,d) the minima of plots obtained in all runs were made the same as that for the solar spectrum.

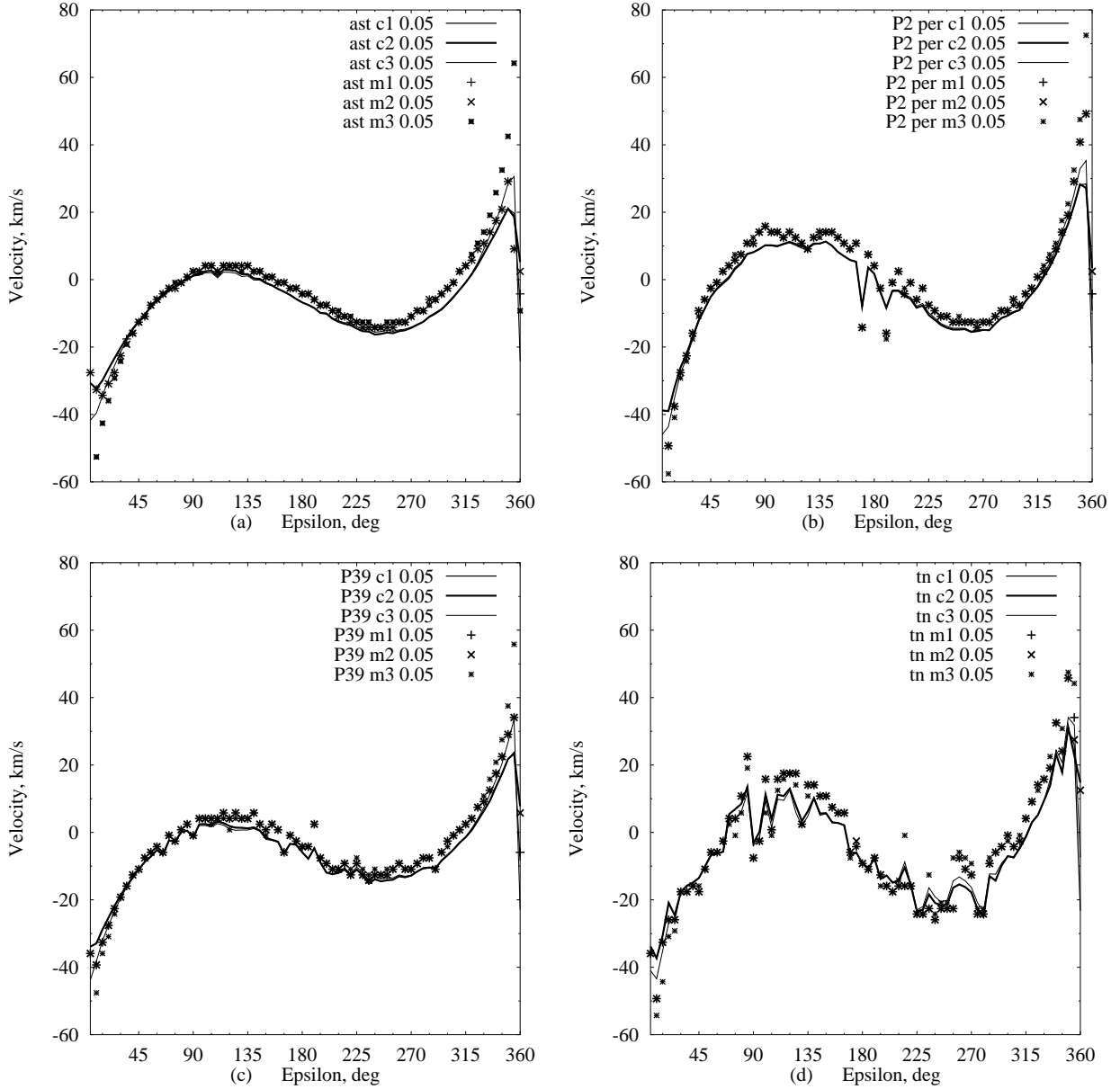


Fig. 2.— Velocities of Mg I line (at zero inclination) versus elongation ϵ (measured eastward from the sun) at $\beta=0.05$ for dust particles started from asteroids (a), Comet 2P at perihelion (b), Comet 39P (c), and trans-Neptunian particles (d). Letter ‘c’ denotes the model for which the shift of the plot of I vs. ϵ is calculated as a shift of centroid, and letter ‘m’ denotes the model for which the shift of the plot is calculated as a shift of the minimum of the plot. The number after ‘m’ or ‘c’ characterizes the number of a scattering function used.

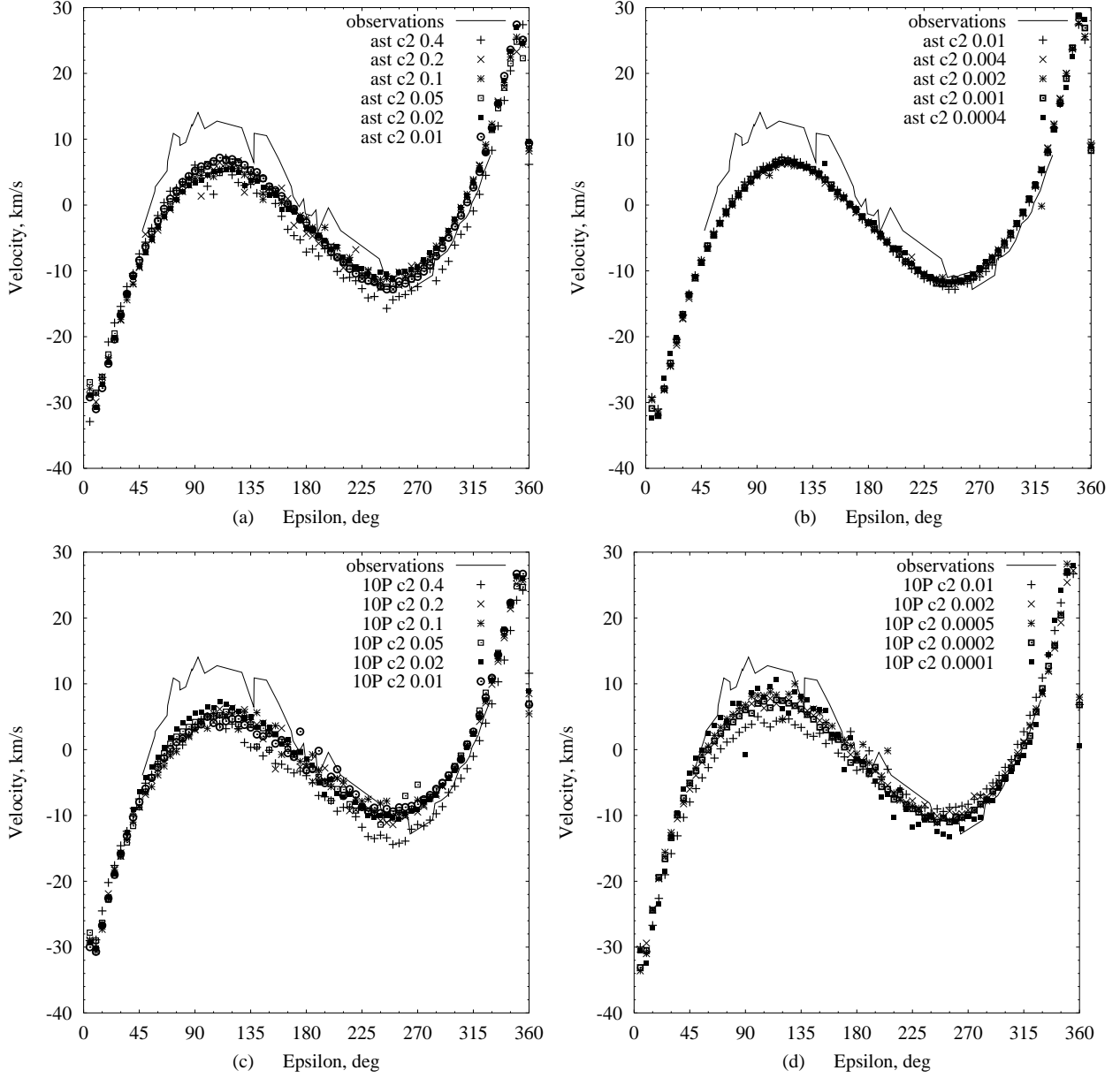


Fig. 3.— Velocities of Mg I line (at zero inclination) versus elongation ϵ (measured eastward from the sun) at several values of β (see the last number in the legend) for particles started from asteroids (a-b) and Comet 10P (c-d). The line corresponds to the observations made by Reynolds et al. (2004).

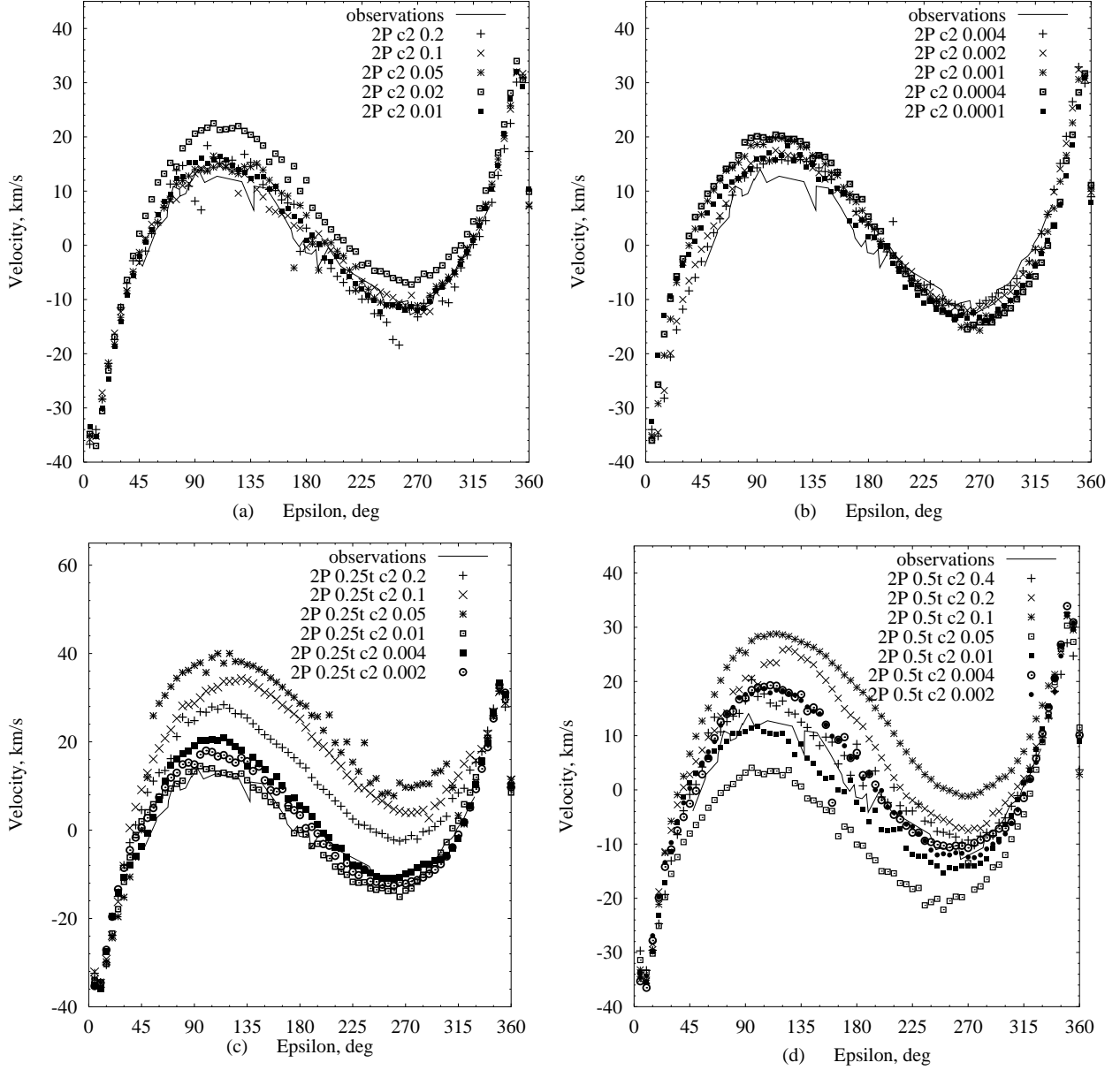


Fig. 4.— Velocities of Mg I line (at zero inclination) versus elongation ϵ (measured eastward from the sun) at several values of β for particles started from Comet 2P at perihelion (a-b), at the middle of the orbit (c), and at aphelion (d). The line corresponds to the observations made by Reynolds et al. (2004).

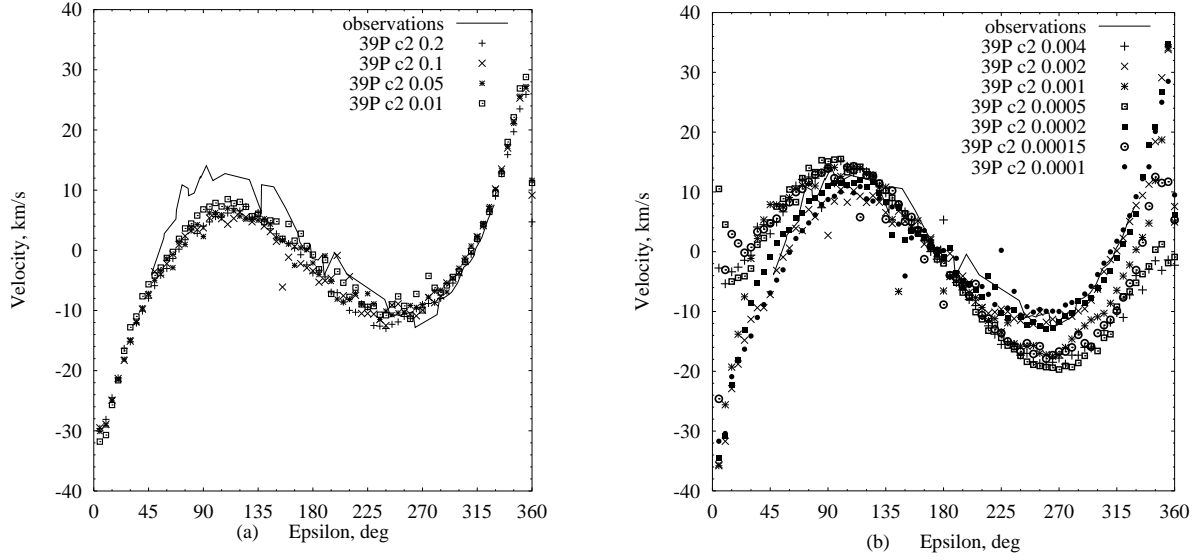


Fig. 5.— Same as Figs. 3-4, but for particles started from Comet 39P.

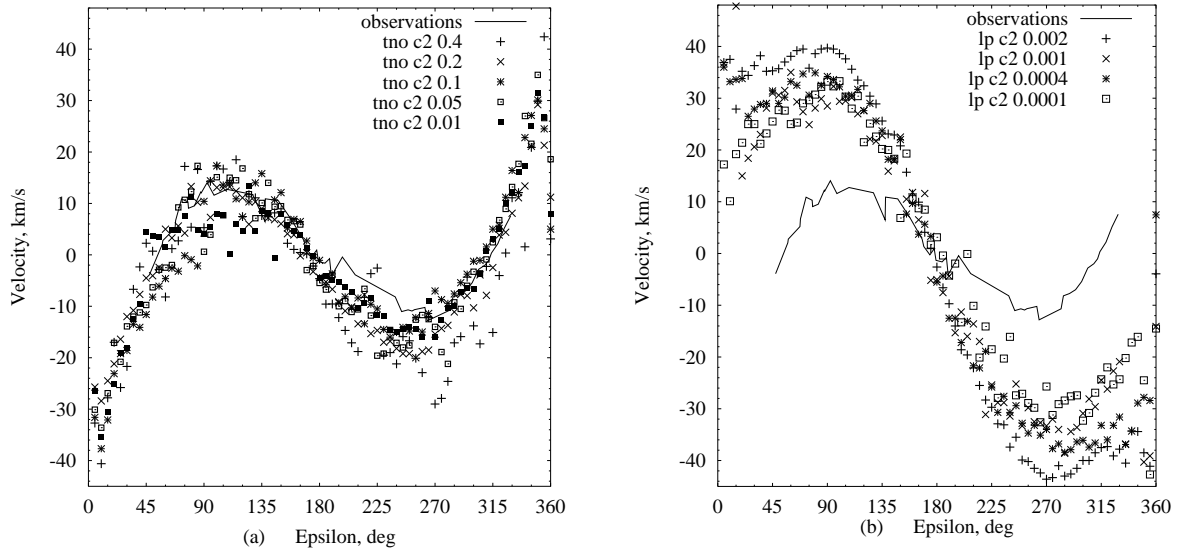


Fig. 6.— Same as Figs. 3-4, but for particles started from trans-Neptunian objects (a) and long-period comets at $e_o=0.995$, $q_o=0.9$ AU, and i_o distributed between 0 and 180° (b).

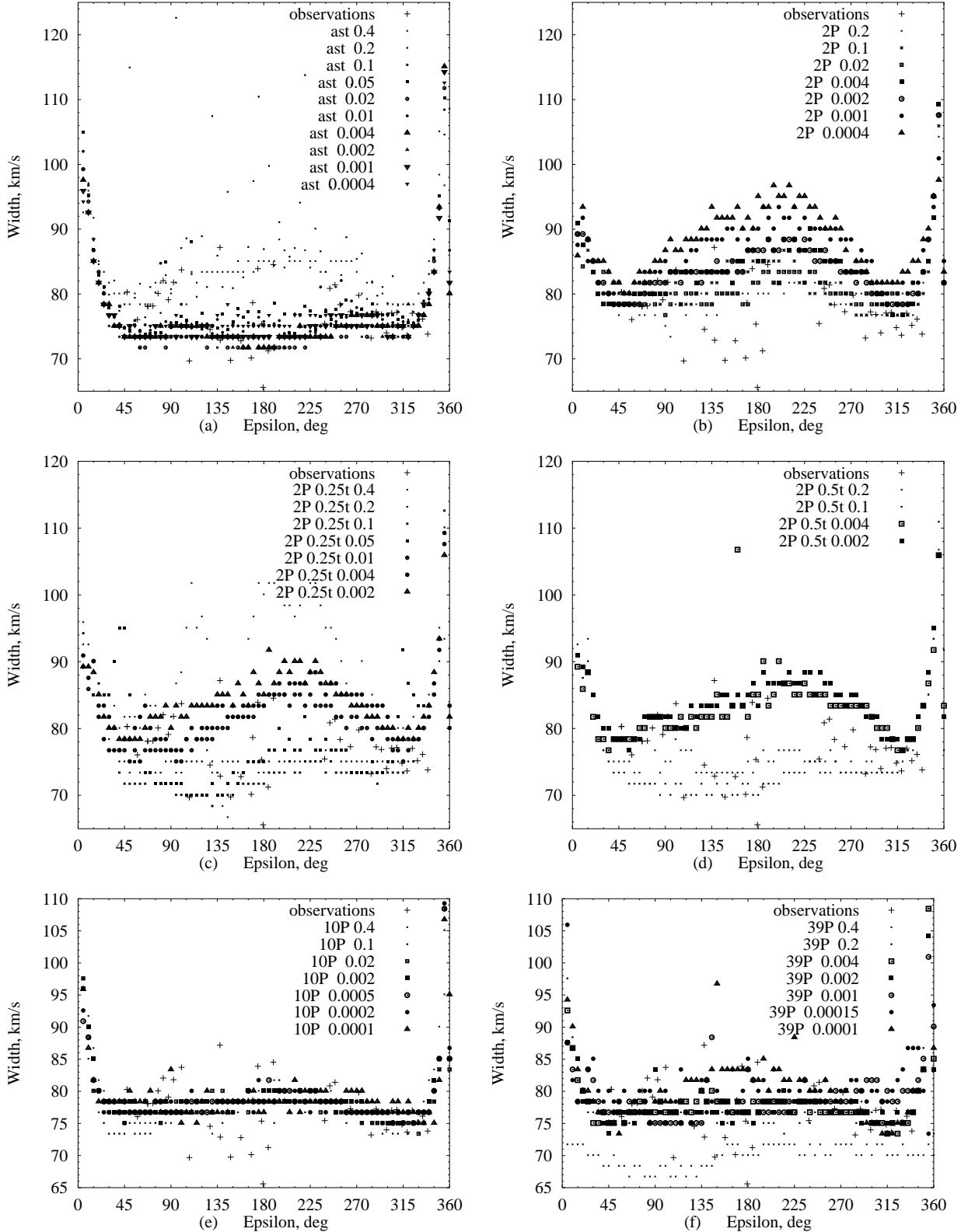


Fig. 7.— Width of Mg I line (in the ecliptic plane) versus elongation ϵ at several values of β for particles started from asteroids (ast), from Comet 2P at perihelion (2P), at the middle of the orbit (2P 0.25t), and at aphelion (2P 0.5t), from Comet 10P (10P), and Comet 39P (39P). The first designation (+) corresponds to the observations made by Reynolds et al. (2004).

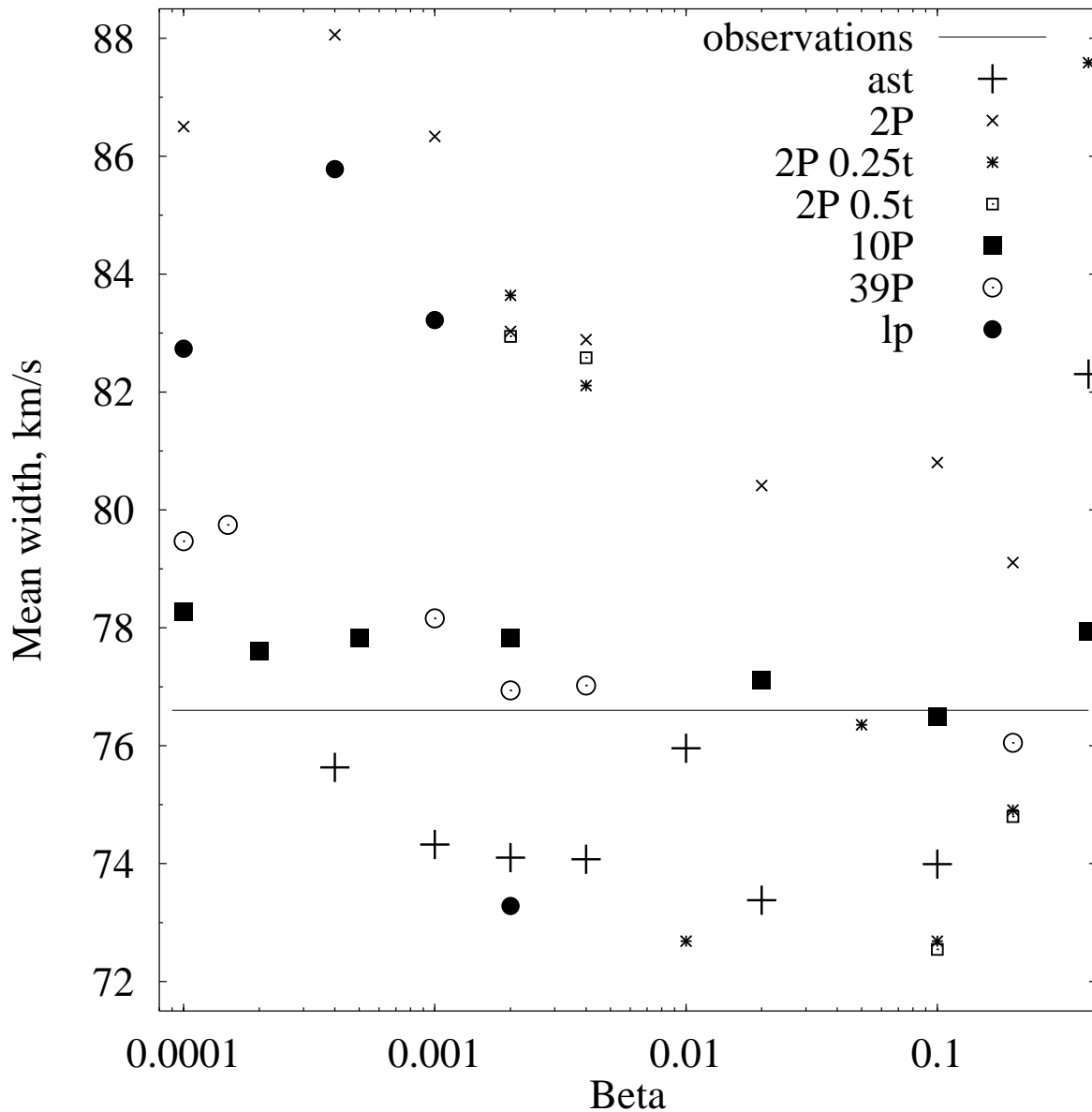


Fig. 8.— Mean value of the width of Mg I line (in the ecliptic plane) for elongation ϵ between 30° and 330° at several values of β for particles started from asteroids (ast), from Comet 2P at perihelion (2P), at the middle of the orbit (2P 0.25t), and at aphelion (2P 0.5t), from Comets 10P and 39P (10P and 39P), and from long-period comets (lp) at $e_o=0.995$, $q_o=0.9$ AU, and i_o distributed between 0 and 180° . Solid line corresponds to the observational value.

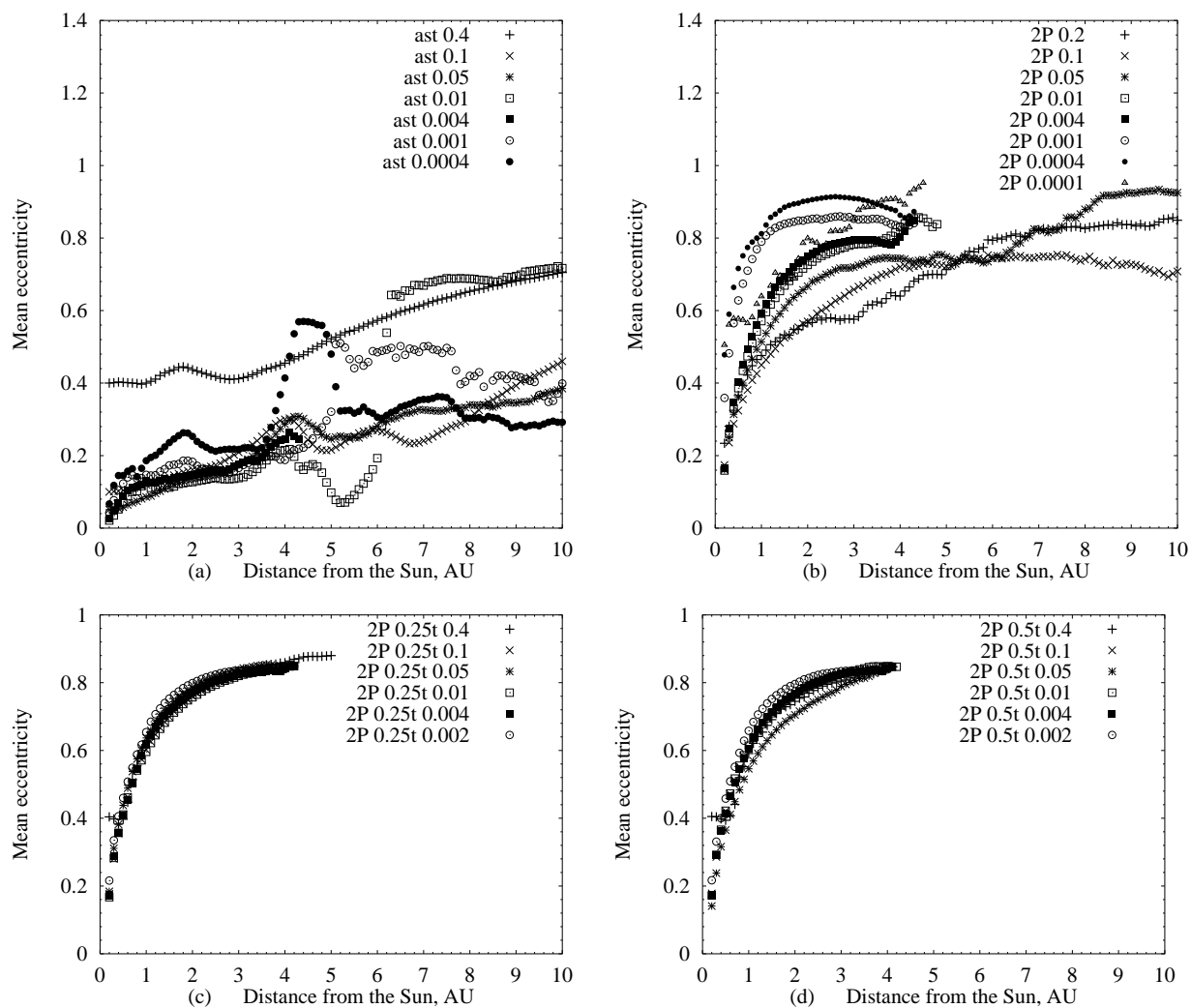


Fig. 9.— Mean eccentricity of particles at different distances from the sun at several values of β (see the last number in the legend) for particles started from asteroids (ast), from Comet 2P at perihelion (2P), at the middle of the orbit (2P 0.25t), and at aphelion (2P 0.5t).

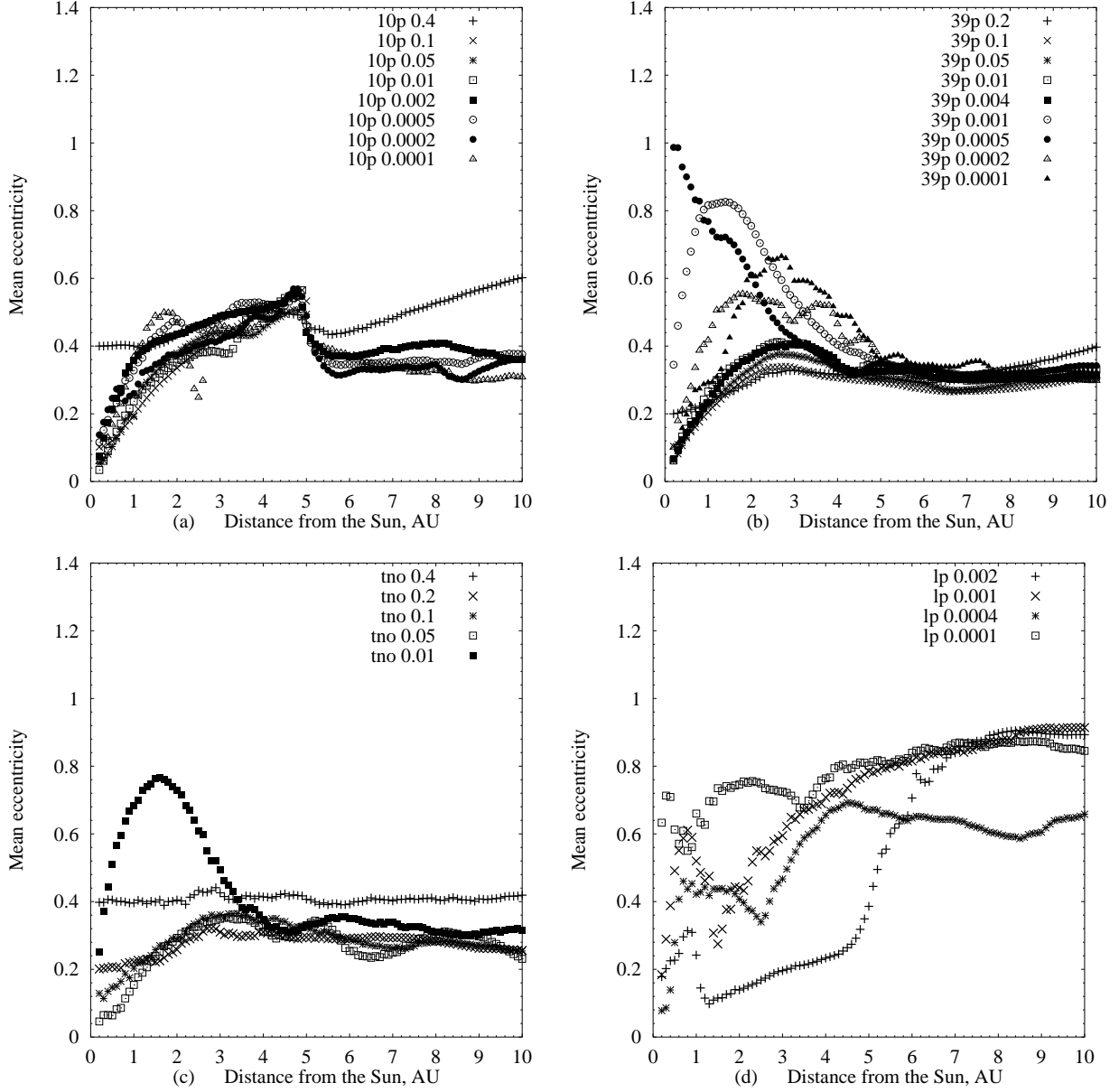


Fig. 10.— Mean eccentricity of particles at different distances from the sun at several values of β (see the last number in the legend) for particles started from Comets 10P and 39P (10P and 39P), from trans-Neptunian objects (tno), and from long-period comets (lp) at $e_o=0.995$, $q_o=0.9$ AU, and i_o distributed between 0 and 180° .

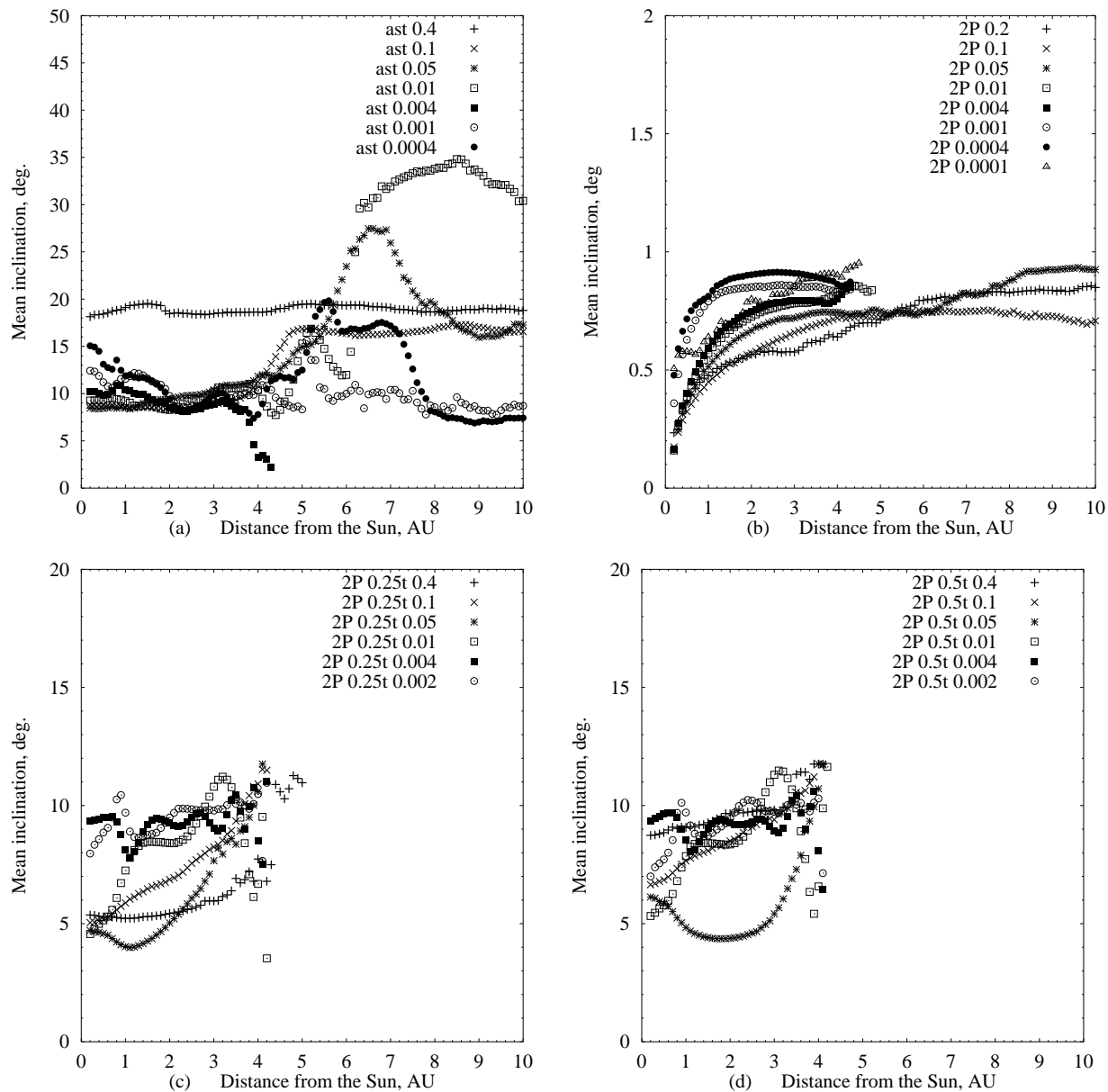


Fig. 11.— Mean orbital inclination (in degrees) of particles at different distances from the sun at several values of β (see the last number in the legend) for particles started from asteroids (ast), from Comet 2P at perihelion (2P), at the middle of the orbit (2P 0.25t), and at aphelion (2P 0.5t).

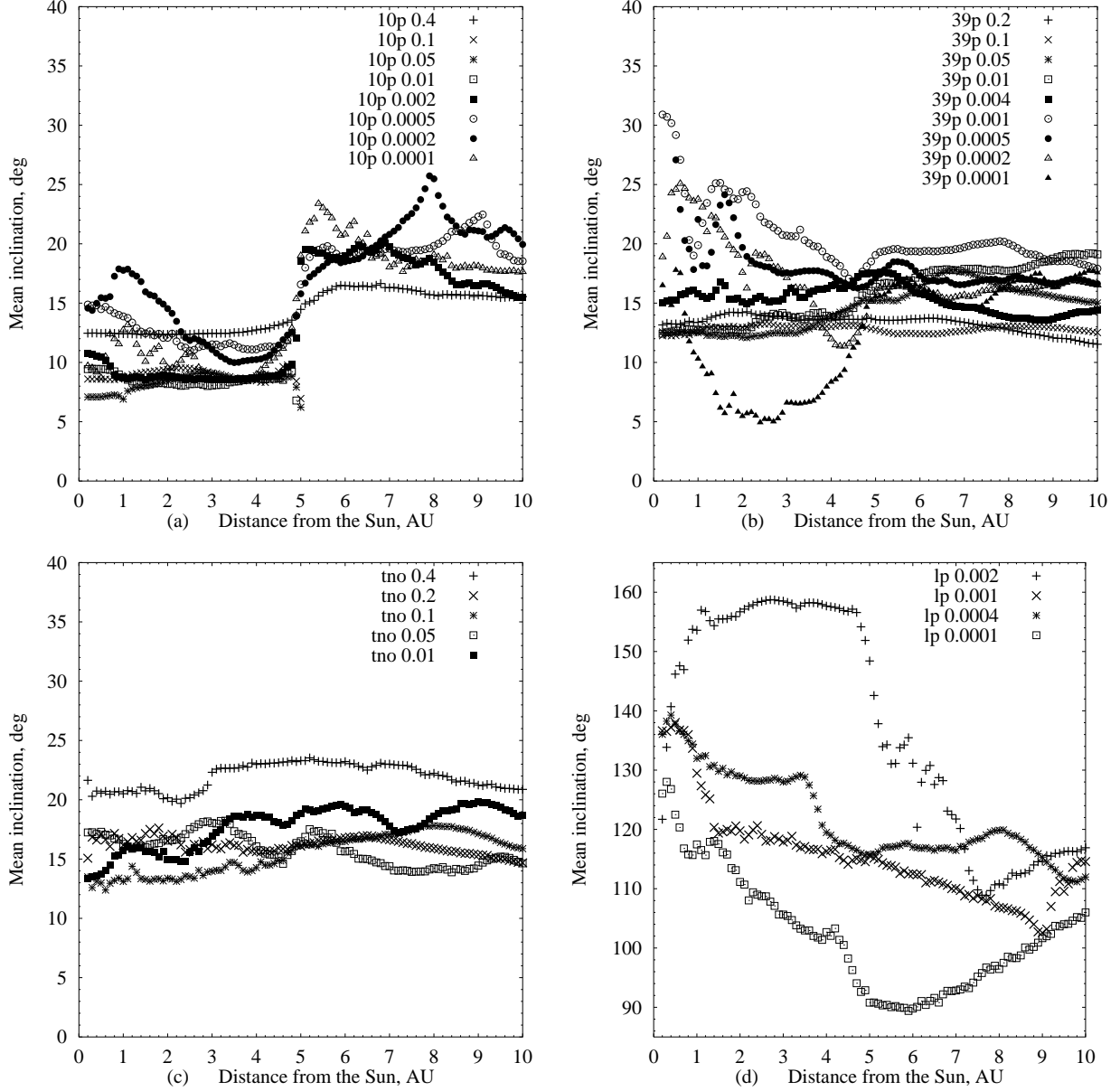


Fig. 12.— Mean orbital inclination (in degrees) of particles at different distances from the sun at several values of β (see the last number in the legend) for particles started from Comets 10P and 39P (10P and 39P), from trans-Neptunian objects (tno), and from long-period comets (lp) at $e_o=0.995$, $q_o=0.9$ AU, and i_o distributed between 0 and 180° .

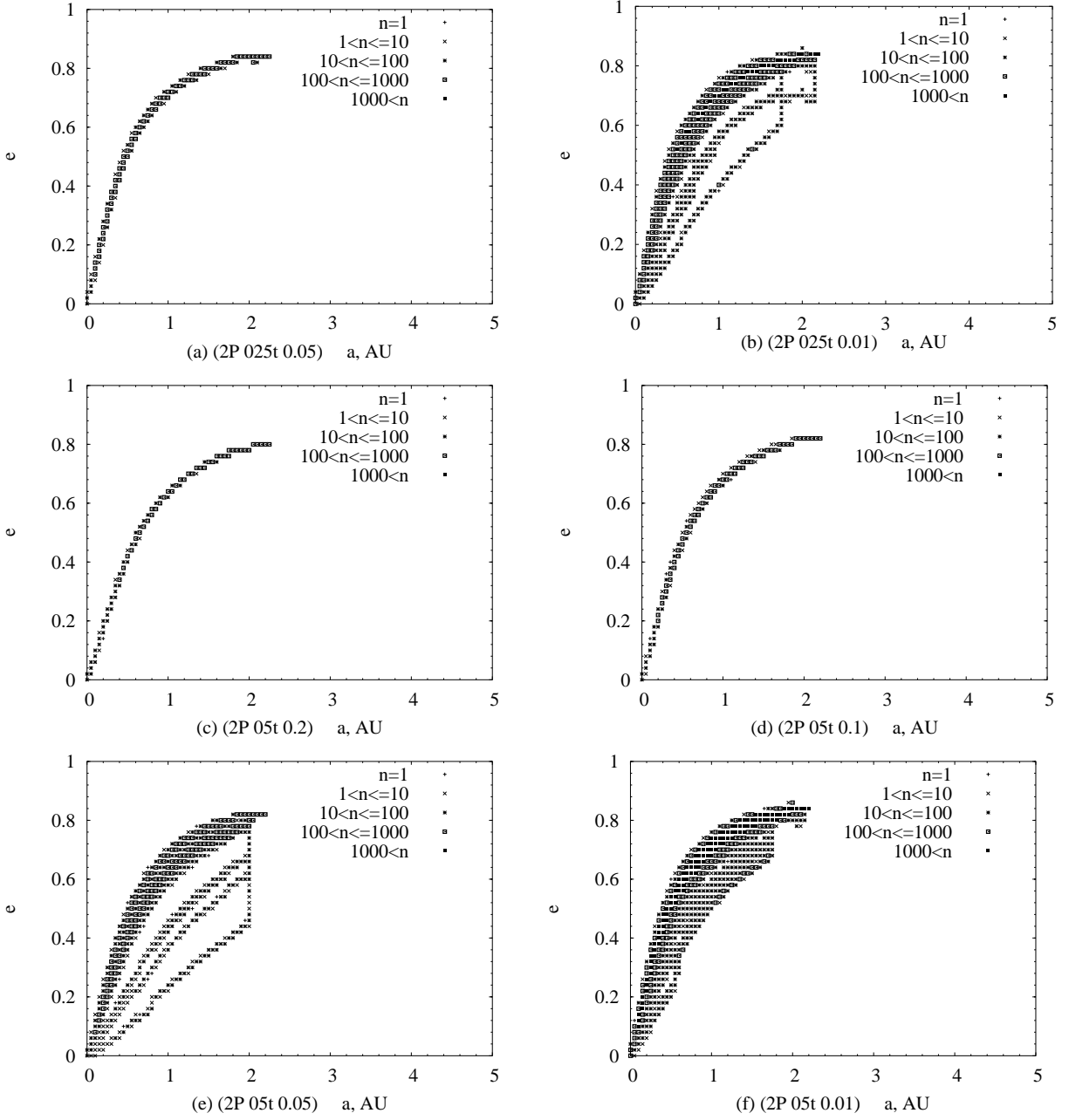


Fig. 13.— Distribution of dust particles with semimajor axis and eccentricity at several values of β (0.05 for (a),(e), 0.01 for (b),(f), 0.2 for (c), and 0.1 for (d)) for particles started from Comet 2P at the middle of the orbit (2P 0.25t) and at aphelion (2P 0.5t). n is the number of orbits with e and a in the interval of width of 0.02 and 0.05 AU, respectively. Orbital elements were stored with a step of 20 yr, and the number of particles in each run was 100 or 250.

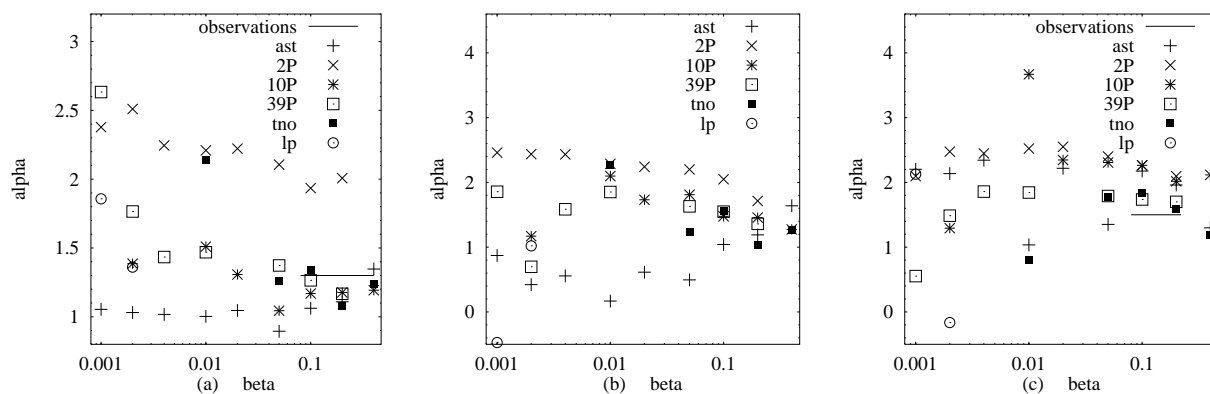


Fig. 14.— Values of α in $n(R) \propto R^{-\alpha}$ obtained by comparison of the values of the number density $n(R)$ at distance R from the sun equal to 0.3 and 1 AU (a), at $R=0.8$ and $R=1.2$ AU (b), and at R equal to 1 and 3 AU (c). The values are presented at several values of β for particles started from Comets 10P and 39P (10P and 39P), from trans-Neptunian objects (tno), and from long-period comets (lp) at $e_o=0.995$, $q_o=0.9$ AU, and i_o distributed between 0 and 180° . Horizontal bars correspond to observations.

Table 1: Characteristic velocity amplitude v_a of ‘velocity-elongation’ curves at $90^\circ < \epsilon < 270^\circ$, minimum (v_{\min}) and maximum (v_{\max}) velocities at the above interval, mean eccentricities (e_z), and mean inclinations (i_z) at distance from the sun $1 \leq R \leq 3$ AU for particles from different sources at intervals of β

Particles	β	e_z	i_z (deg.)	v_a (km s ⁻¹)	v_{\min} (km s ⁻¹)	v_{\max} (km s ⁻¹)
asteroidal	0.0004-0.1	<0.3	8-13	9	(-13)-(-11)	5-7
10P	0.0001-0.2	0.2-0.5	7-18	8	(-11)-(-9)	3-9
39P	0.01-0.2	0.2-0.4	12-15	8-9	(-13)-(-9)	4-8
39P	0.0001-0.004	0.28-0.82	5-25	11-17	(-20)-(-10)	8-16
2P	0.01-0.1	0.45-0.85	0.45-0.8	13	(-12)-(-7)	12-22
2P	0.0001-0.004	0.6-0.9	0.6-0.9	14	(-16)-(-12)	15-20
2P 0.25t	0.002-0.2	0.6-0.85	4-11	16	(-14)-4	12-40
2P 0.5t	0.002-0.4	0.55-0.85	4-11	14	(-22)-(-2)	2-29
tno	0.05-0.4	0.15-0.45	13-22	16	(-20)-(-14)	12-18
tno	0.01	0.48-0.76	14-17	12	-16	8
lp, $q=0.9$ AU	0.002	0.1-0.25	154-160	41	-44	38
lp, $q=0.9$ AU	0.0001-0.001	0.28-0.76	105-132	33	(-38)-(-32)	28-34
lp, $q=0.1$ AU	0.0004	0.44-0.55	104-113	34	-34	34